

# Recent BES results and the BESIII upgrade

*F. A. Harris*

*for the BES Collaboration*

Department of Physics and Astronomy

University of Hawaii

Honolulu, HI 96822

USA

## Abstract

Using 58 million  $J/\psi$  and 14 million  $\psi(2S)$  events collected by the BESII detector at the BEPC, branching fractions or upper limits for the decays  $J/\psi$  and  $\psi(2S) \rightarrow \Lambda\bar{\Lambda}\pi^0$  and  $\Lambda\bar{\Lambda}\eta$  are measured, and the decays of  $J/\psi$  and  $\psi(2S)$  to  $nK_S^0\bar{\Lambda} + c.c.$  are observed and measured for the first time. Finally,  $R$  measurement data taken with the BESII detector at center-of-mass energies between 3.7 and 5.0 GeV are fitted to determine resonance parameters of the high mass charmonium states,  $\psi(3770)$ ,  $\psi(4040)$ ,  $\psi(4160)$ , and  $\psi(4415)$ .

The Beijing Electron Collider is being upgraded to a two-ring collider (BEPCII) with a design luminosity of  $1 \times 10^{33} \text{cm}^{-2} \text{s}^{-1}$  at 3.89 GeV and will operate between 2 and 4.2 GeV in the center of mass. With this luminosity, the new BESIII detector will be able to collect, for example, 10 billion  $J/\psi$  events in one year of running. BEPCII and BESIII are currently nearing completion, and commissioning of both is expected to begin in mid-2008.

## 1 Introduction

In this paper, some recent BESII results are reported based on 58 million  $J/\psi$  and 14 million  $\psi(2S)$  events collected by the BESII detector at the BEPC, and the status of BESIII/BEPCII is summarized. For much more detail, see the references.

## 2 Recent Results

### 2.1 $J/\psi$ and $\psi(2S)$ decays into $\Lambda\bar{\Lambda}\pi^0$ and $\Lambda\bar{\Lambda}\eta$

The isospin violating decay  $J/\psi \rightarrow \Lambda\bar{\Lambda}\pi^0$  was studied by DM2 [1] and BES I [2], and its average branching fraction is  $\mathcal{B}(J/\psi \rightarrow \Lambda\bar{\Lambda}\pi^0) = (2.2 \pm$

Table 1: Measured branching fractions or upper limits at the 90% confidence level (C.L.).

Channels	Number of events	MC efficiency (%)	Branching fraction ( $\times 10^{-4}$ )
$J/\psi \rightarrow \Lambda \bar{\Lambda} \pi^0$	$< 11.2$	0.75	$< 0.64$
$J/\psi \rightarrow \Lambda \bar{\Lambda} \eta$	$44 \pm 10$	1.8	$2.62 \pm 0.60 \pm 0.44$
$\psi(2S) \rightarrow \Lambda \bar{\Lambda} \pi^0$	$< 7.0$	2.5	$< 0.49$
$\psi(2S) \rightarrow \Lambda \bar{\Lambda} \eta$	$< 7.6$	2.9	$< 1.2$
$J/\psi \rightarrow \Sigma^+ \pi^- \bar{\Lambda}$	$335 \pm 22$	2.3	$7.70 \pm 0.51 \pm 0.83$
$J/\psi \rightarrow \bar{\Sigma}^- \pi^+ \Lambda$	$254 \pm 19$	1.8	$7.47 \pm 0.56 \pm 0.76$

$0.6) \times 10^{-4}$  [3]. However, the isospin conserving process  $J/\psi \rightarrow \Lambda \bar{\Lambda} \eta$  has not been reported, and there are no measurements for  $\Lambda \bar{\Lambda} \pi^0$  and  $\Lambda \bar{\Lambda} \eta$  decays of  $\psi(2S)$ .

Here  $J/\psi \rightarrow \Lambda \bar{\Lambda} \pi^0$ ,  $J/\psi \rightarrow \Lambda \bar{\Lambda} \eta$ ,  $\psi(2S) \rightarrow \Lambda \bar{\Lambda} \pi^0$ , and  $\psi(2S) \rightarrow \Lambda \bar{\Lambda} \eta$ , where  $\Lambda$  decays to  $\pi^- p$  and  $\pi^0$  and  $\eta$  to  $\gamma\gamma$ , are studied. Candidate events must have four good charged tracks and at least two photons, two protons identified using particle identification, a satisfactory four constraint kinematic fit, and a  $\pi p$  mass consistent with the  $\Lambda$  mass. For  $J/\psi \rightarrow \Lambda \bar{\Lambda} \pi^0$ , the decay lengths of  $\Lambda$  and  $\bar{\Lambda}$  in the  $x - y$  plane must be larger than 0.05 m.

Possible backgrounds are studied using MC simulation. The most serious one is from  $J/\psi \rightarrow \Sigma^0 \pi^0 \bar{\Lambda} + c.c.$ , which contains  $\Lambda \bar{\Lambda} \pi^0$  with an additional photon in the final state. The branching fraction for this decay has not been previously measured. Since direct measurement of  $J/\psi \rightarrow \Sigma^0 \pi^0 \bar{\Lambda} + c.c.$  is difficult, we measure the branching fractions of its isospin partner and estimate the branching fraction assuming isospin symmetry.

The histogram in Fig. 1 shows normalized backgrounds from all background channels, and the dashed line in the figure shows the  $\pi^0$  signal from MC simulated  $J/\psi \rightarrow \Lambda \bar{\Lambda} \pi^0$ . The data in Fig. 1 are consistent with background, and the upper limit on the number of  $\pi^0$  events from  $J/\psi \rightarrow \Lambda \bar{\Lambda} \pi^0$  is determined. Figure 2 shows the  $\gamma\gamma$  invariant mass distribution for  $J/\psi \rightarrow \Lambda \bar{\Lambda} \eta$  candidates, where a clear  $\eta$  signal is observed. Figure 3 shows the  $\gamma\gamma$  invariant mass distribution for  $\psi(2S) \rightarrow \Lambda \bar{\Lambda} \pi^0$  and  $\Lambda \bar{\Lambda} \eta$  using similar selection criteria, and no significant  $\pi^0$  or  $\eta$  signals are seen.

Table 1 lists the results for  $J/\psi$  and  $\psi(2S)$  decay into  $\Lambda \bar{\Lambda} \pi^0$  and  $\Lambda \bar{\Lambda} \eta$ , as well as  $J/\psi \rightarrow \Sigma^+ \pi^- \bar{\Lambda} + c.c.$ . Except for  $J/\psi \rightarrow \Lambda \bar{\Lambda} \pi^0$  and  $J/\psi \rightarrow \Sigma^+ \pi^- \bar{\Lambda} + c.c.$ , the results are first measurements. Interestingly, the result of  $J/\psi \rightarrow \Lambda \bar{\Lambda} \pi^0$  presented here is much smaller than those of DM2 and BES1 [1,2]. Previously, the large contaminations from  $J/\psi \rightarrow \Sigma^0 \pi^0 \bar{\Lambda} + c.c.$

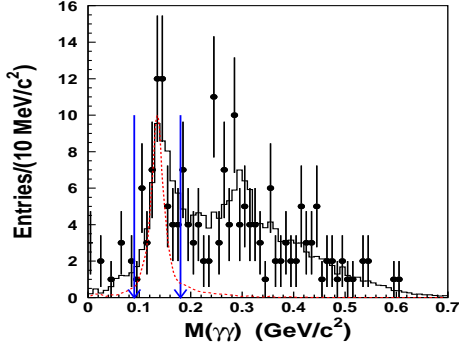


Figure 1: Invariant mass distribution of  $M(\gamma\gamma)$  for  $J/\psi \rightarrow \Lambda\bar{\Lambda}\pi^0 \rightarrow \Lambda\bar{\Lambda}\gamma\gamma$  candidates (dots with error bars) and normalized backgrounds (solid histogram). The dashed curves shows the  $\pi^0$  signal from MC simulated  $J/\psi \rightarrow \Lambda\bar{\Lambda}\pi^0$ .

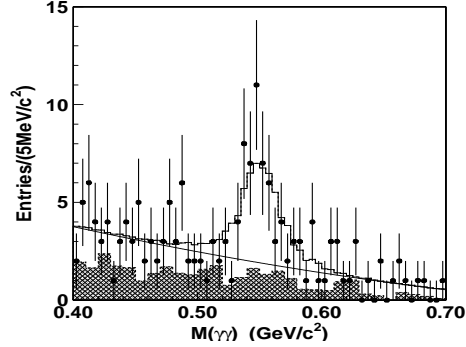


Figure 2: Fit to the  $\gamma\gamma$  invariant mass distribution of  $J/\psi \rightarrow \Lambda\bar{\Lambda}\eta \rightarrow \Lambda\bar{\Lambda}\gamma\gamma$  candidate events. Dots with error bars are data, the hatched histogram is the normalized background, and the solid histogram is the fit to data using a histogram of the signal shape from MC simulation plus a second order polynomial for background.

and  $J/\psi \rightarrow \Sigma^+\pi^-\bar{\Lambda} + c.c.$  were not considered, resulting in a large  $J/\psi \rightarrow \Lambda\bar{\Lambda}\pi^0$  branching fraction. The small branching fraction of  $J/\psi \rightarrow \Lambda\bar{\Lambda}\pi^0$  and relatively large branching fraction of  $J/\psi \rightarrow \Lambda\bar{\Lambda}\eta$  measured here indicate that the isospin violating decay in  $J/\psi$  decays is suppressed while the isospin conserving decays is favored, which is consistent with expectation. For more detail, see Ref. [4].

## 2.2 $J/\psi$ and $\psi(2S)$ decaying to $nK_S^0\bar{\Lambda} + c.c.$

In 2004, BESII reported the observation of an enhancement  $X(2075)$  near the threshold of the invariant mass spectrum of  $p\bar{\Lambda}$  in  $J/\psi \rightarrow pK^-\bar{\Lambda}$  decays. The mass, width, and product branching fraction of this enhancement are  $M = 2075 \pm 12$  (stat.)  $\pm 5$  (syst.) MeV/ $c^2$ ,  $\Gamma = 90 \pm 35$  (stat.)  $\pm 9$  (syst.) MeV/ $c^2$ , and  $B(J/\psi \rightarrow K^-X)B(X \rightarrow p\bar{\Lambda} + c.c.) = (5.9 \pm 1.4 \pm 2.0) \times 10^{-5}$  [5], respectively. The study of the isospin conjugate channel  $J/\psi \rightarrow nK_S^0\bar{\Lambda}$  is therefore important not only in exploring new decay modes of  $J/\psi$  but also in understanding the  $X(2075)$ .

$J/\psi$  and  $\psi(2S) \rightarrow nK_S^0\bar{\Lambda}$  with  $K_S^0 \rightarrow \pi^+\pi^-$  and  $\bar{\Lambda} \rightarrow \bar{p}\pi^+$  (and *c.c.*) final states contain four charged tracks and an undetected neutron or anti-neutron.

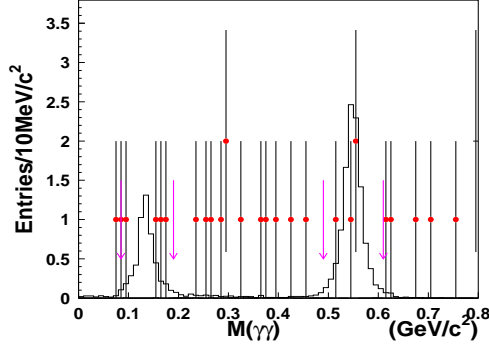


Figure 3: The  $\gamma\gamma$  invariant mass distribution for candidate  $\psi(2S) \rightarrow \gamma\gamma\Lambda\bar{\Lambda}$  events. Dots with error bars are data, and the histograms are MC simulated signal events. The arrows indicate the  $\pi^0$  and  $\eta$  signal regions.

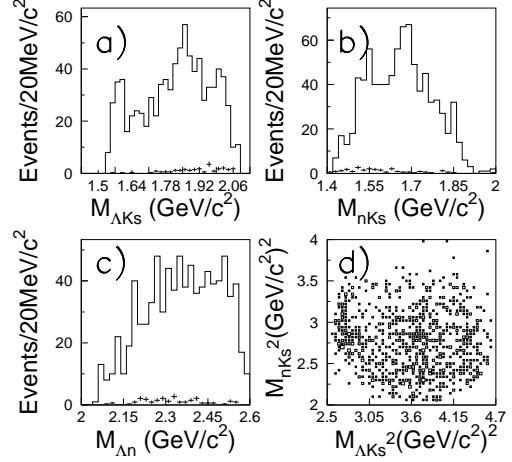


Figure 4: The invariant mass spectra of (a)  $\Lambda K_S^0$ , (b)  $nK_S^0$ , and (c)  $\bar{\Lambda}n(\Lambda\bar{n})$ , as well as (d) the Dalitz plot for candidate  $J/\psi \rightarrow nK_S^0\Lambda + c.c.$  events after all selection criteria. The crosses show the sideband backgrounds.

We require the candidate events to have four charged tracks with total charge zero. Secondary vertex fitting is used to identify the  $\pi^+\pi^-$  from the  $K_S^0$  and the  $p\pi$  from the  $\Lambda$ , and their masses are required to be consistent with those of the parent particles. To reject backgrounds from channels without a  $K_S^0$  or  $\Lambda$ , we require  $L_{xy}(\Lambda)$ , the distance from the reconstructed  $\Lambda$  vertex to the event origin, to be larger than 5 mm and  $L_{xy}(K_S^0) > 5$  mm. To suppress background and improve the resolution, a one constraint (1C) kinematic fit with a missing neutron is applied under the  $J/\psi \rightarrow \bar{p}n\pi^+\pi^-\pi^+$  hypothesis, and  $\chi_{1C}^2 < 5$  is required.

The invariant mass spectra of  $\Lambda K_S^0$ ,  $nK_S^0$ , and  $\bar{\Lambda}n(\Lambda\bar{n})$ , as well as the Dalitz plot for all selection requirements are shown in Fig. 4. In the  $\Lambda K_S^0$  invariant mass spectrum, an enhancement near  $\Lambda K_S^0$  threshold is evident, as is found in the  $\Lambda K$  mass spectrum in  $J/\psi \rightarrow pK^-\bar{\Lambda}$  [6]. The  $X(2075)$  signal which was seen in the  $p\bar{\Lambda}$  invariant mass spectrum in  $J/\psi \rightarrow pK^-\bar{\Lambda}$  is not significant here. Taking into account the systematic error, the upper limit of the near-threshold enhancement  $X(2075)$  in the  $n\bar{\Lambda}$  threshold is  $B(J/\psi \rightarrow K_S^0 X(2075)) \cdot B(X(2075) \rightarrow n\bar{\Lambda}) < 4.9 \times 10^{-5}$  (90% C.L.). Considering

the isospin factor, the branching fraction upper limit for  $B(J/\psi \rightarrow K_S^0 X) \cdot B(X \rightarrow n\bar{\Lambda} + c.c.)$  is not inconsistent with that for  $B(J/\psi \rightarrow KX) \cdot B(X \rightarrow p\bar{\Lambda} + c.c.)$  [5].

An  $N^*$  state at around 1.9 GeV/c<sup>2</sup> in the  $\Lambda K_S^0$  invariant mass spectrum and  $\Lambda^*$  states at around 1.5 and 1.7 GeV/c<sup>2</sup> in the  $nK_S^0$  invariant mass spectrum are present. A larger data sample and a partial wave analysis are needed to analyze these states.

We use the same criteria to select  $\psi(2S) \rightarrow nK_S^0\bar{\Lambda} + c.c.$  events from the BESII sample of 14M  $\psi(2S)$  events. The branching ratios obtained are:

$$\begin{aligned} Br(J/\psi \rightarrow nK_S^0\bar{\Lambda} + c.c.) &= (6.46 \pm 0.20 \pm 1.07) \times 10^{-4} \\ Br(J/\psi \rightarrow nK_S^0\bar{\Lambda}) &= (3.09 \pm 0.14 \pm 0.58) \times 10^{-4} \\ Br(J/\psi \rightarrow \bar{n}K_S^0\Lambda) &= (3.39 \pm 0.15 \pm 0.48) \times 10^{-4} \\ Br(\psi(2S) \rightarrow nK_S^0\bar{\Lambda} + c.c.) &= (0.81 \pm 0.11 \pm 0.14) \times 10^{-4}. \end{aligned}$$

The ratio of the branching ratios of  $\psi(2S)$  and  $J/\psi$  decaying to  $nK_S^0\bar{\Lambda} + c.c.$ ,  $Q_h = (12.6 \pm 3.5)\%$ , obeys the "12%" rule [7]. For more detail, see Ref. [8].

### 2.3 $\psi(3770)$ , $\psi(4040)$ , $\psi(4160)$ and $\psi(4415)$ resonance parameters

The total cross section for hadron production in  $e^+e^-$  annihilation is usually parameterized in terms of the ratio  $R$ , which is defined as  $R = \sigma(e^+e^- \rightarrow \text{hadrons})/\sigma(e^+e^- \rightarrow \mu^+\mu^-)$ , where the denominator is the lowest-order QED cross section,  $\sigma(e^+e^- \rightarrow \mu^+\mu^-) = \sigma_{\mu\mu}^0 = 4\pi\alpha^2/3s$ . At the open flavor thresholds where resonance structures show up,  $R$  measurements are used to determine resonance parameters. For the high mass charmonium resonances, the  $\psi(3770)$  was measured by MARK-I [9], DELCO [10], MARK-II [11] and BES [12] [13]; the  $\psi(4040)$  and  $\psi(4160)$  were measured by DASP [14]; and the  $\psi(4415)$  was measured by DASP [14] and MARK-I [15].

The most recent and precise  $R$  measurements between 2-5 GeV were made by BESII [16]. Experimentally,  $R$  for both the continuum and the wide resonance region is given by

$$R_{exp} = \frac{N_{had}^{obs} - N_{bg}}{\sigma_{\mu\mu}^0 L \epsilon_{trg} \epsilon_{had} (1 + \delta_{obs})}, \quad (1)$$

where  $N_{had}^{obs}$  is the number of observed hadronic events,  $N_{bg}$  is the number of the residual background events,  $L$  is the integrated luminosity,  $(1 + \delta_{obs})$  is the effective correction factor of the initial state radiation (ISR) [17] [18],  $\epsilon_{had}$  is the detection efficiency for hadronic events determined by Monte Carlo

Table 2: The resonance parameters of the high mass charmonia in this work together with the values in PDG2004 [19], PDG2006 [3] and K. Seth's evaluations [20] based on Crystal Ball and BES data.

		$\psi(3770)$	$\psi(4040)$	$\psi(4160)$	$\psi(4415)$
$M$ (MeV/ $c^2$ )	PDG2004	$3769.9 \pm 2.5$	$4040 \pm 10$	$4159 \pm 20$	$4415 \pm 6$
	PDG2006	$3771.1 \pm 2.4$	$4039 \pm 1.0$	$4153 \pm 3$	$4421 \pm 4$
	CB (Seth)	-	$4037 \pm 2$	$4151 \pm 4$	$4425 \pm 6$
	BES (Seth)	-	$4040 \pm 1$	$4155 \pm 5$	$4455 \pm 6$
	BES (this work)	$3771.4 \pm 1.8$	$4038.5 \pm 4.6$	$4191.6 \pm 6.0$	$4415.2 \pm 7.5$
$\Gamma_{tot}$ (MeV)	PDG2004	$23.6 \pm 2.7$	$52 \pm 10$	$78 \pm 20$	$43 \pm 15$
	PDG2006	$23.0 \pm 2.7$	$80 \pm 10$	$103 \pm 8$	$62 \pm 20$
	CB (Seth)	-	$85 \pm 10$	$107 \pm 10$	$119 \pm 16$
	BES (Seth)	-	$89 \pm 6$	$107 \pm 16$	$118 \pm 35$
	BES (this work)	$25.4 \pm 6.5$	$81.2 \pm 14.4$	$72.7 \pm 15.1$	$73.3 \pm 21.2$
$\Gamma_{ee}$ (keV)	PDG2004	$0.26 \pm 0.04$	$0.75 \pm 0.15$	$0.77 \pm 0.23$	$0.47 \pm 0.10$
	PDG2006	$0.24 \pm 0.03$	$0.86 \pm 0.08$	$0.83 \pm 0.07$	$0.58 \pm 0.07$
	CB (Seth)	-	$0.88 \pm 0.11$	$0.83 \pm 0.08$	$0.72 \pm 0.11$
	BES (Seth)	-	$0.91 \pm 0.13$	$0.84 \pm 0.13$	$0.64 \pm 0.23$
	BES (this work)	$0.18 \pm 0.04$	$0.81 \pm 0.20$	$0.50 \pm 0.27$	$0.37 \pm 0.14$
$\delta$ (degree)	BES (this work)	0	$133 \pm 68$	$301 \pm 61$	$246 \pm 86$

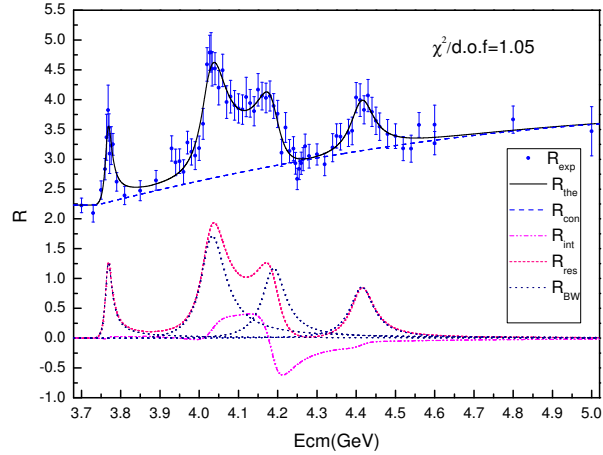


Figure 5: The fit to the  $R$  values in the high mass charmonium region. The dots with error bars are the updated  $R$  values. The solid curve shows the best fit, and the other curves show the contributions from each resonance  $R_{BW}$ , the interference  $R_{int}$ , the summation of the four resonances  $R_{res} = R_{BW} + R_{int}$ , and the continuum background  $R_{con}$  respectively.

simulation without bremsstrahlung being simulated, and  $\epsilon_{trg}$  is the trigger efficiency.

In the previous analysis [16], the determination of  $R$  values was done using PDG04 [19] resonance parameters for the high mass resonances. Here, the analysis uses the data to determine the resonance parameters. The determination of  $R$  values and resonance parameters are intertwined; the factor  $(1 + \delta_{obs})$  in Eq. (1) contains contributions from the resonances and depends on the resonance parameters. Therefore, the procedure to calculate  $(1 + \delta_{obs})$  requires a number of iterations before stable results can be obtained. We perform a global fit over the entire center-of-mass energy region from 3.7 to 5.0 GeV covering the four resonances,  $\psi(3770)$ ,  $\psi(4040)$ ,  $\psi(4160)$  and  $\psi(4415)$ , and include interference effects among the resonances. We also adopt energy-dependent full widths, and introduce relative phases between the resonances.

The resonant parameters of the high mass charmonia determined in this work, together with those in PDG2004, PDG2006 and the results given in Ref. [20] are listed in Table 2. The updated  $R$  values between 3.7 and 5.0 GeV and the fit curves are illustrated in Fig. 5.

It is worth noting that the change of the resonance parameters affects the effective initial state radiative correction factors, and thus affects the  $R$  values. In general the relative difference is within 3%, and for a few energy points the maximum difference is about 6%. Our resonance parameter results are in agreement with the previous experiments in most cases, but large differences are observed in some of the parameters, such as the mass of the  $\psi(4160)$ . This is mainly due to the reconsideration of the radiative correction factors, and the inclusion of interferences between the resonances. This work is preliminary; for more detail, see Ref. [21].

### 3 BEPCII and BESIII

In 2003, the Chinese Government approved the upgrade of the BEPC to a two-ring collider (BEPCII) with a design luminosity approximately 100 times higher than that of the BEPC. This will allow unprecedented physics opportunities in this energy region and contribute to precision flavor physics.

#### 3.1 BEPCII

BEPCII is a two-ring  $e^+e^-$  collider that will run in the tau-charm energy region ( $E_{cm} = 2.0 - 4.2$  GeV) with a design luminosity of  $1 \times 10^{33}$  cm<sup>-2</sup>s<sup>-1</sup> at a beam energy of 1.89 GeV, an improvement of a factor of 100 with respect

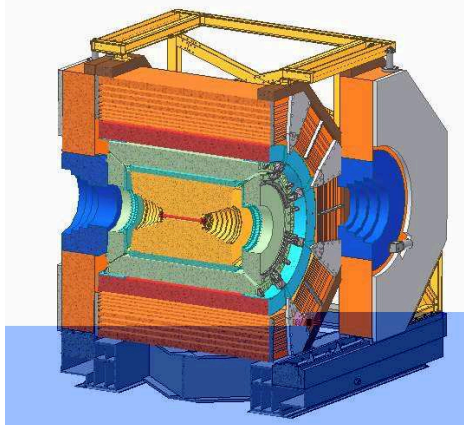


Figure 6: Schematic view of the BESIII detector.

to the BEPC. This is accomplished by using multi-bunches and micro-beta. The upgrade uses the existing tunnel.

The 2024 meter long linac has been upgraded with new klystrons, a new electron gun, and a new positron source to increase its energy and beam current; it can accelerate electrons and positrons up to 1.89 GeV with a positron injection rate of 50 mA/min. Its installation was completed in the summer of 2005.

There are two storage rings with lengths of 237.5 meters. The collider has new super-conducting RF cavities, power supplies, and control; super-conducting quadrupole magnets; beam pipes; magnets and power supplies; kickers; beam instrumentation; vacuum systems; and control. The old dipoles are modified and used in the outer ring. Electrons and positrons will collide at the interaction point with a horizontal crossing angle of 11 mrad and bunch spacing of 8 ns. Each ring has 93 bunches with a beam current of 9170 mA. The machine is already providing a high flux of synchrotron radiation at a beam energy of 2.5 GeV.

### 3.2 BESIII

The BESIII detector consists of a beryllium beam pipe, a helium-based small-celled drift chamber, Time-Of-Flight counters for particle identification, a CsI(Tl) crystal calorimeter, a super-conducting solenoidal magnet with a field of 1 Tesla, and a muon identifier using the magnet yoke interleaved with Resistive Plate Counters (RPC). Fig. 6 shows the schematic view of the BESIII detector, including both the barrel and endcap portions.

### 3.3 Physics in the tau-charm energy region

The tau-charm energy region makes available a wide variety of interesting physics. Data can be taken at the  $J/\psi$ ,  $\psi(2S)$ , and  $\psi(3770)$ , at  $\tau$  threshold, and at an energy to allow production of  $D_s$  pairs, as well as for an R-scan.

Table 3: Number of events expected for one year of running.

Physics channel	Center-of-mass Energy (GeV)	Peak Luminosity ( $10^{33} \text{ cm}^{-2} \text{ s}^{-1}$ )	Physics cross section (nb)	Number of Events per year
$J/\psi$	3.097	0.6	$\sim 3400$	$10 \times 10^9$
$\tau$	3.67	1.0	$\sim 2.4$	$12 \times 10^6$
$\psi(2S)$	3.686	1.0	$\sim 640$	$3.0 \times 10^9$
$D$	3.770	1.0	$\sim 5$	$25 \times 10^6$
$D_s$	4.030	0.6	$\sim 0.32$	$1.0 \times 10^6$
$D_s$	4.140	0.6	$\sim 0.67$	$2.0 \times 10^6$

BEPCh and BESIII are in the final stage of assembly, and commissioning will begin in summer 2008. The design luminosity of BESIII is  $1 \times 10^{33} \text{ cm}^{-2}$ . Clearly BESIII with higher luminosity will contribute greatly to precision flavor physics:  $V_{cd}$  and  $V_{cs}$  will be measured with a statistical accuracy of 1.6%.  $D^0 D^0$  mixing will be studied and CP violation will be searched for. Table 3 gives the numbers of events expected during one year of running at various energies. Huge  $J/\psi$  and  $\psi(2S)$  samples will be obtained. The  $\eta_C$ ,  $\chi_{CJ}$ , and  $h_C$  can be studied with high statistics, and the  $\rho\pi$  puzzle will be studied with better accuracy. For more detail, see Refs [22, 23].

## 4 References

### References

- [1] P. Henrard *et al.* [DM2 Collab.], *Nucl. Phys. B* **292**, 670 (1987).
- [2] J. Z. Bai *et al.* [BES Collab.], *Phys. Lett. B* **424**, 213 (1998).
- [3] W. M. Yao *et al.* [Particle Physics Group], *J. Phys.* **G 33**, 1 (2006).
- [4] M. Ablikim *et al.* [BES Collab.], *Phys. Rev. D* **76**, 092003 (2007).
- [5] M. Ablikim *et al.* [BES Collab.], *Phys. Rev. Lett.* **93**, 112002 (2004).

- [6] Shan JIN for the BES Collab., *Int. J. Mod. Phys. A* **21**, 613 (2006).
- [7] T. Appelquist and H. D. Politzer, *Phys. Rev. Lett.* **34**, 43 (1975); A. De Rujula and S. L. Glashow, *ibid*, page 46.
- [8] M. Ablikim *et al.* [BES Collab.], accepted by *Phys. Lett. B*, arXiv:0710.3091 [hep-ex].
- [9] P. A. Rapidis *et al.* [MARK-I Collab.], *Phys. Rev. Lett.* **39**, 526 (1977).
- [10] W. Bacino *et al.* [DELCO Collab.], *Phys. Rev. Lett.* **40**, 671 (1978).
- [11] R. H. Schindler *et al.* [MARK-II Collab.], *Phys. Rev. D* **21**, 2716 (1980).
- [12] M. Ablikim *et al.* [BES Collab.], *Phys. Lett. B* **652**, 238 (2007).
- [13] M. Ablikim *et al.* [BES Collab.], *Phys. Rev. Lett.* **97**, 121801 (2006).
- [14] R. Brandelik *et al.* [DASP Collab.], *Phys. Lett. B* **76**, 361 (1978).
- [15] J. Siegrist *et al.* [MarkI Collab.], *Phys. Rev. Lett.* **36**, 700, (1976).
- [16] J. Z. Bai *et al.* [BES Collab.], *Phys. Rev. Lett.* **88**, 101802 (2002).
- [17] A. Osterfeld *et al.* [Crystal Ball Collab.], Report No. SLAC-PUB-4160 (1986) (unpublished).
- [18] H. M. Hu *et al.*, *High Energy Physics and Nuclear Physics* **25**, 701 (2001) (in Chinese).
- [19] S. Eidelman *et al.* [Particle Data Group], *Phys. Lett. B* **592**, 310 (2004).
- [20] K. K. Seth, *Phys. Rev. D* **72**, 017501 (2005).
- [21] M. Ablikim *et al.* [BES Collab.], submitted to *Phys. Lett. B*, arXiv:0705.4500 [hep-ex].
- [22] F. A. Harris, *Nucl. Phys. Proc. Suppl.* **162**, 345 (2006).
- [23] Weiguo Li, to be published in the Proceedings of 4th Flavor Physics and CP Violation Conference, hep-physics/0605158.